THE JOURNAL OF PHYSICAL CHEMISTRY Letters

Letter

pubs.acs.org/JPCL

Free-Energy Barriers and Reaction Mechanisms for the Electrochemical Reduction of CO on the Cu(100) Surface, Including Multiple Layers of Explicit Solvent at pH 0

Tao Cheng, Hai Xiao, and William A. Goddard, III*

Materials and Process Simulation Center, California Institute of Technology, Pasadena, California 91125, United States

Supporting Information

ABSTRACT: The great interest in the photochemical reduction from CO_2 to fuels and chemicals has focused attention on Cu because of its unique ability to catalyze formation of carbon-containing fuels and chemicals. A particular goal is to learn how to modify the Cu catalysts to enhance the production selectivity while reducing the energy requirements (overpotential). To enable such developments, we report here the *free-energy reaction barriers* and *mechanistic pathways* on the Cu(100) surface, which produces only CH_4 (not C_2H_4 or CH_3OH) in acid (pH 0). We predict a threshold potential for CH_4 formation of −0.52 V, which compares well to experiments at low pH, −0.45 to −0.50 V. These *quantum molecular dynamics* simulations included ∼5 layers of *explicit water* at the water/electrode interface using enhanced sampling methodology to obtain the free energies. We find that that chemisorbed hydroxyl-methylene (CH−OH) is the key intermediate determining the selectivity for methane over methanol.

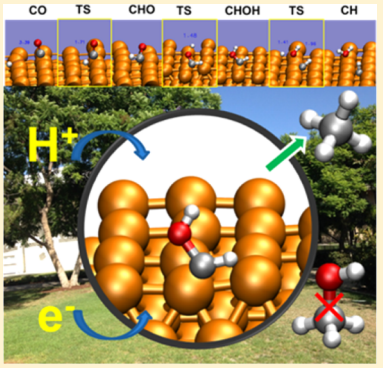

Electrochemically reducing CO_2 to fuels and organic feedstocks could provide a means for converting this greenhouse gas to valuable products.[1−6] Ever since Hori made his landmark discovery in 1985,[7] Cu metal remains the only metal catalyst able to convert CO_2 to hydrocarbons; however, the efficiency of this CO_2 reduction reaction (CO_2RR) is far too low to be commercially useful. Although the thermodynamic potential to produce CH_4 is +0.17 V vs standard hydrogen electrode (SHE), Cu requires a potential of about −0.8 V vs reversible hydrogen electrode (RHE) at pH ≈ 7 for the onset of CH_4 production from CO_2 (the overpotential is −0.45 to −0.50 V at pH 1.0).[8] Moreover, overpotential of −1.0 V (RHE) is required for a reasonable current of 2 mA/cm^{-2} at pH ≈ 7, which is attributed to sluggish kinetics of CO_2 reduction reactions and competition with hydrogen evolution reactions (HERs).[9−12] In addition, Cu leads to poor selectivity toward valuable products,[13] although the enhanced selectivity for nanoscale Cu catalysts suggests that these properties of Cu might be improved.[14−16]

To provide a basis for rational design of catalysts to achieve more efficient CO2RR,[17,18] we focus here on obtaining a full understanding of the reaction mechanisms responsible for CO2RR on Cu. Experiments have shown that the CO reduction reaction (CORR) leads to products and overpotential similar to those of CO2RR, indicating that the potential determining step (PDS) is due to CORR.[8] Several reaction mechanisms for CORR have been hypothesized based on experimental observations.[19−22] However, it has not yet been possible to observe the reaction intermediates experimentally so that the steps determining the selectivity and rates of methane (CH_4) over methanol (CH_3OH) are not known. Instead we will use quantum mechanics (QM) to determine the free-energy barriers for each possible reaction step while including explicit solvent at pH 0.

The first full investigation of C1 productions (CH_4 and CH_3OH) on Cu was reported by Peterson et al.,[23,24] who proposed the reaction mechanism in eq 1 for CH_4 formation on the Cu(211) surface:

$$CO^* \xrightarrow{H^*} CHO^* \xrightarrow{H^*} CH_2O^* \xrightarrow{H^*} CH_3O^* \xrightarrow{H^*} CH_4 + O^* \quad (1)$$

In this pathway, CHO formation is PDS controlling the overall overpotential. They explained the observed selectivity of CH_4 over CH_3OH as occurring in the final step ($CH_3O^* \xrightarrow{H^*} CH_3OH(aq)$ vs $CH_3O^* \xrightarrow{H^*} CH_4 + O^*$). They argued that CH_4 is formed instead of CH_3OH because CH_4 + O* has a free energy lower than that of CH_3OH. In these calculations the energies (or free energies after correcting for entropy and solvation) were the only criteria, with no calculation of reaction barriers and only a crude estimate of solvation. The assumption was that reaction energy barriers would follow linear free-energy relationships.

The first QM calculations that considered reaction barriers (with one to two explicit water molecules) were reported by Nie et al., who considered CO2RR on the Cu(111) surface.[25] In contrast to Peterson et al, they found that the first step of CO reduction is to form COH instead of formyl (CHO), because on the Cu(111) surface the energy barrier for forming

Received: October 8, 2015
Accepted: November 12, 2015
Published: November 12, 2015

DOI: 10.1021/acs.jpclett.5b02247
J. Phys. Chem. Lett. 2015, 6, 4767−4773

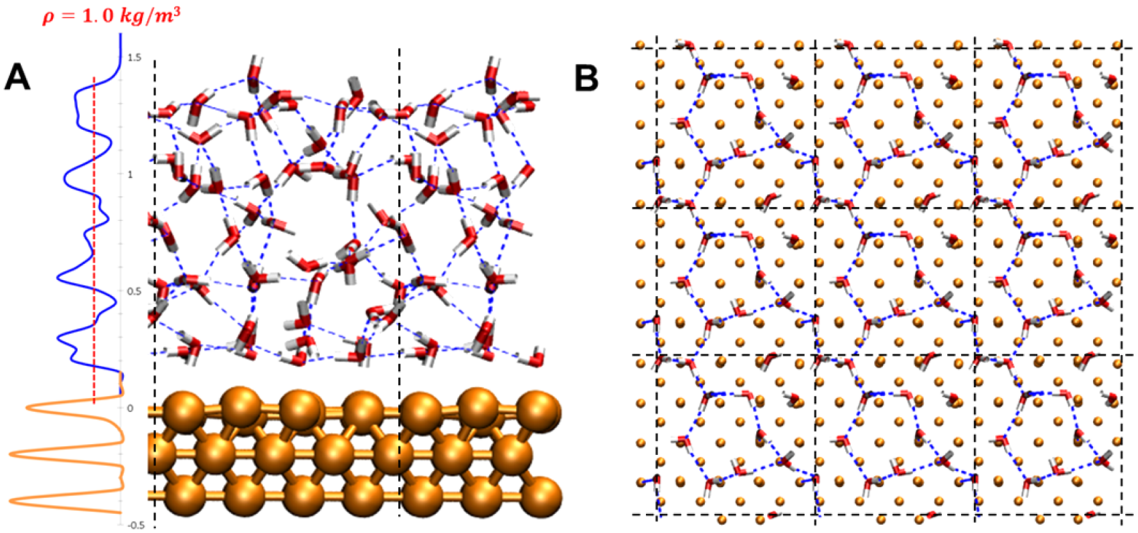

Figure 1. Water/Cu(100) interface from side view (A) and first layer water on Cu(100) from top view (B). About five layers of water can be distinguished based on the density profile shown on the left of panel A. (The unit of density profile is kilograms per cubic meter for Cu (orange) and water (blue), with Cu scaled down by 10 times; the red slashed line shows the density of bulk water (1.0 kg/m^3) at room temperature.) Panel B shows the water molecules belonging to the first layer. There are 12 water molecules on this 4 × 4 surface, corresponding to coverage of 3/4 ML. The atom colors are Cu in orange, O in red, and H in white. HBs are indicated with blue dashed lines based on cut-offs of 3.5 Å for distance and 35° for angle (OH bond away from the O−O line). Black slashed lines show the boundary of the simulation cell.

COH (0.21 eV) is much smaller than for CHO (0.39 eV), although the chemisorbed species differ only by an energy of 0.12 eV. Thus, Nie proposed the following reduction mechanism:

$$CO^* \xrightarrow{H^*} COH^* \xrightarrow{H^*} C \xrightarrow{H^*} CH \xrightarrow{H^*} CH_2^* \xrightarrow{H^*} CH_3^* \xrightarrow{H^*} CH_4 \quad (2)$$

Nie also calculated the pathway for CH_4 formation proposed by Peterson et al. for Cu(211) but concluded that this pathway produces CH_3OH instead of CH_4 on Cu(111), consistent with gas-phase experiments.[26]

Based on these postulated reaction mechanisms, computational screening was used to propose new alloy or nanostructured catalysts.[27−30]

Recent experiments showed that under standard electrochemical conditions polycrystalline Cu transforms in 30 min to Cu(111) followed by transforming to Cu(100) after 60 min, remaining as Cu(100) for the duration.[31] This is consistent with experiments showing that polycrystalline Cu leads to products similar to Cu(100). Consequently, we focus here on the Cu(100) surface.

Moreover, Cu(100) is a more active surface than Cu(111), leading to lower onset overpotentials for both CH_4 formation and C_2H_4 formation.[8] The relative selectivity toward C_2H_4 over CH_4 is unclear. Earlier work by Hori and co-workers showed a strong structural dependence: CH_4 is preferentially formed on Cu(111), while C_2H_4 is the main product on Cu(100).[32] In addition, recent research found a strong pH dependence of the product selectivity; thus, at pH 1 (acidic), CH_4 is observed[8] but not C_2H_4 or other C2 products both on Cu(100) and Cu(111). In contrast, C_2H_4 production is comparable with CH_4 production for neutral and basic solutions.[8] A pH-dependent mechanism for CH_4 formation was hypothesized on the basis of these experimental data but never validated experimentally or theoretically.[8]

In this paper we focus on acid conditions (pH 0) to determine the reaction mechanisms and barriers using quantum molecular dynamics (QMD) with 3 layers of 4 × 4 periodic cell of Cu(100) (48 Cu atoms with the bottom two layers fixed), 49 H_2O molecules, one of which is protonated, with two CO molecules and one H atom bound to the surface. This leads to ∼6 layers of explicit water at pH 0 to describe the CO reduction at the water/Cu(100) interface.

We applied enhanced sampling methodology [QM-based constrained molecular dynamics (CMD) and meta-dynamics][33−37] to drive the chemical reactions to sample the reaction barrier configurations not normally sampled in brute force MD simulations. The predicted free-energy differences and free-energy barriers explicitly include solvent and entropy effects. The QM is at the PBE level of density functional theory with D3 vdW correction; other simulation details are in the Supporting Information.

Allowing the low-frequency movements involved in relaxing the hydrogen bond (HB) network for the solvent in contact with the metal interface requires 100−200 ps, which is too long for practical QMD. Thus, we first used the reactive force field molecular dynamics simulation (RMD) of the full water/Cu(100) system for 500 ps to equilibrate the system at 298 K.[38,39] Starting with this equilibrated configuration from RMD, we selected ∼5 layers of solvent, minimized the structure using QM, and then heated it using QMD from 50 to 298 K over 2 ps (125 K/ps).Then we equilibrated the system using QMD in the *NVT* ensemble at 298 K to form the initial state for free-energy calculations, which takes ∼5 ps. The convergence behaviors for these calculations are shown in the Supporting Information (Figure S1).

Figure 1 shows the structure of water at the Cu(100) interface obtained from QMD simulations. This structure is quite different from the bulk, being much less ordered than that observed for (111) and (110)[40−45] metal surfaces, but there are few studies on (100) surfaces.[46] The first contact layer of water consists of a loosely packed HB network with many dangling OH, as shown in Figure 1B, a snapshot of the water in the first contact layer after equilibration. About 12 water molecules belong to the first layer, leading to a surface concentration of 3/

DOI: 10.1021/acs.jpclett.5b02247
J. Phys. Chem. Lett. 2015, 6, 4767−4773

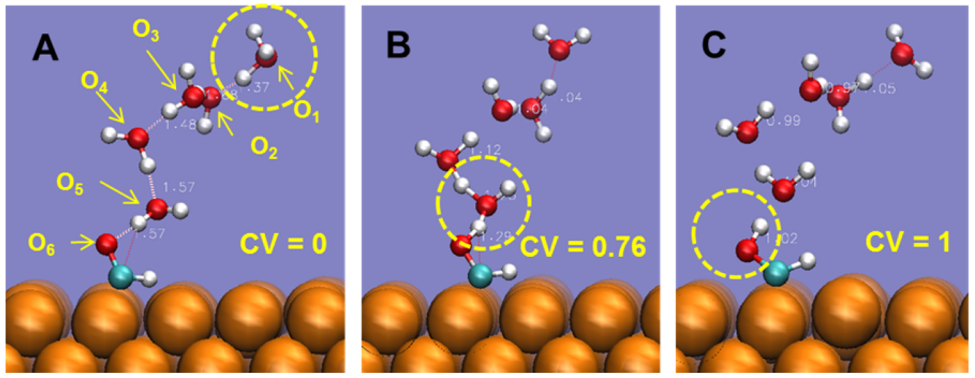

Figure 2. HB network connecting H_3O^+ and CHO* for reaction R2a. Such collective modes are typically observed for protonation reactions in solvents.[49] The collective variable defined here is the HB network: $\xi = (\sum_{i=1}^{5} r_{O_{i+1}-H_i}^{2})^{1/2}$. This HB network was used as the collective variable to describe the reaction from $H_3O^+ + e^- +$ CHO* (A) to CHOH* (C). The transition state is shown in panel B. The colors of atoms are Cu in orange, O in red, H in white, and C in cyan.

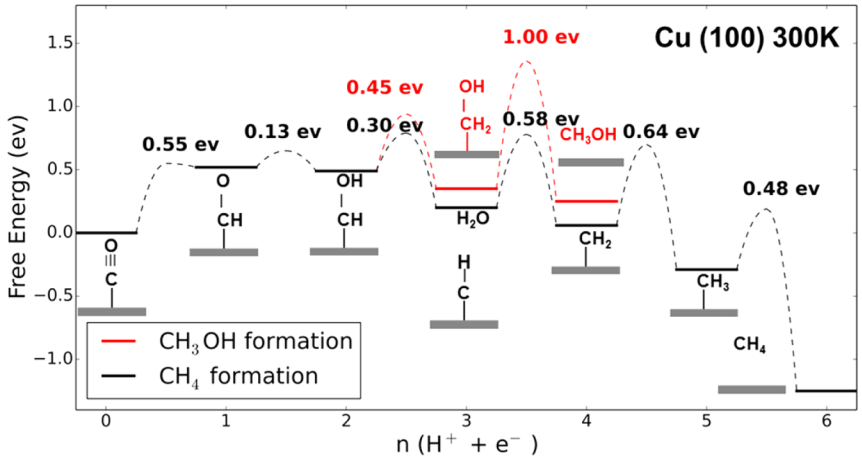

Figure 3. Lowest-energy pathways for the electro-reduction of CO to methane on Cu(100) at pH 0 (CH_4, in black) and methanol (CH_3OH, in red). The free-energy reaction barriers ($\Delta G^{\ddagger}$) are provided. This shows that only CH_4 will be produced under these conditions, as observed experimentally.

4 ML, which is larger than the nominal concentration for water on a close-packed flat metal surface (2/3 ML).[42] This is because the (100) surface has an area per surface atom 15% larger than that of the (111) surface. The density profile in Figure 1 shows five layers of water with a thickness of about 1.5 nm. The first two density peaks result from the OH-up, OH-down, and OH parallel configurations in the first contact layer. These two peaks together with the third peak describe the double-layer region on the surface, which extends to about 0.7 nm from the Cu surface. Beyond the double layer to ∼1.2 nm, the density fluctuates about the bulk value. Finally, the gas−liquid interface is ∼1.4−1.5 nm from the surface. Because all reactions take place in the first two layers, we consider this to be an adequate representation for the surface reactions.

To describe the reduction reactions, we included two CO molecules on the Cu(100) surface (coverage of 1/8 ML). CO adsorption prefers the top site on the Cu(100) surface (shown in Figure 2) with a calculated binding energy of 1.24 eV at the PBE level using the D3 vdW correction.[47] We also included one H on the surface (1/16 ML), which prefers the 4-fold hollow site, very close to the surface. We added one H to one of the 49 H_2O molecules, leading effectively to H_3O^+ because the electron goes to the metal, leading to 1.2 M or pH ≈ 0. Simulations using only neutral H_2O solvent lead to an electron chemical potential of −4.07 eV, while changing one H_3O^+ increases the electron chemical potential to −3.57 eV. An additional hydrogen atom was added to the simulation system after each reduction reaction. The 500 ps of ReaxFF RMD led to the H_3O in the third layer, where it stayed during the QM RMD. Because the total number of electrons in our QMD simulations is constant, the work function on the Cu slab changes as the H^+ of this H_3O^+ is involved in reactions. To compare with the constant potential of experiments, we used the procedure proposed by Chan and Nørskov[48] to remove any artifacts involving work function changes during the chemical reactions, as explained in the Supporting Information.

We used enhanced sampling methods, constrained molecular dynamics,[33,34,37] and meta-dynamics[35,36] to drive the chemical reactions to obtain **the free-energy profile along reaction paths** defined by collective variables (CV). The theoretical background for these methods has been published.[35,37] In proton-transfer reactions, the reaction pathways may involve multidimensions, which can become computationally impractical for CMD. Instead we define an appropriate CV utilizing the HB network to connect the proton to the reactant so that CMD one-dimensional samplings can be described using one CV reaction. The CV for reaction R2a is shown in Figure 2.

DOI: 10.1021/acs.jpclett.5b02247
J. Phys. Chem. Lett. 2015, 6, 4767−4773

Table 1. Free-Energy Differences (ΔG) and Free-Energy Barriers ($\Delta G^{\ddagger}$) for Various Reduction Steps of CORR on Cu(100)[a]

H(N)	Reactions	$\Delta G^{\ddagger}$ (ev)	ΔG (ev)
1a	$\boldsymbol{CO^* + H^* \rightarrow CHO^*}$	**0.55(0.09)**	**0.52(0.10)**
1b	$CO^* + H^* \rightarrow COH^*$	1.45(0.10)	1.08(0.11)
1c	$CO^* + H_3O^+ + e^- \rightarrow COH^* + H_2O(aq)$	0.70(0.07)	0.68(0.07)
1d	$CO^* + H_2O^* \rightarrow COH^* + OH^*$	0.74(0.11)	0.72(0.11)
2a	$\boldsymbol{CHO^* + H_3O^+ + e^- \rightarrow CHOH^*}$	**0.13(0.06)**	**-0.03(0.05)**
2b	$CHO^* + H_2O^* \rightarrow CHOH^* + OH^*$	0.24(0.09)	0.13(0.08)
2c	$CHO^* + H^* \rightarrow CH_2O^*$	0.59(0.07)	-0.02(0.08)
3a	$\boldsymbol{CHOH^* + H_3O^+ + e^- \rightarrow CH^* + H_2O(aq)}$	**0.30(0.09)**	**-0.21(0.09)**
3b	$CHOH^* + H_3O^+ + e^- \rightarrow CH\cdots H_2O^*$	0.32(0.05)	0.24(0.06)
3b$^{\text{dehydration}}$	$CH\cdots H_2O^* \rightarrow CH^* + H_2O^*(aq)$	0.21(0.06)	-0.44(0.08)
3c	$CHOH^* + H^* \rightarrow CH_2OH^*$	0.45(0.04)	0.04(0.05)
4a	$CH^* + H^* \rightarrow CH_2^*$	0.58(0.07)	-0.14(0.08)
4b	$CH_2OH + H^* \rightarrow CH_3OH^*$	1.00(0.08)	-0.10(0.09)
5	$CH_2^* + H^* \rightarrow CH_3^*$	0.64(0.07)	-0.35(0.08)
6	$CH_3^* + H^* \rightarrow CH_4^*$	0.48(0.11)	-0.96(0.11)
HER	$H_3O^+ + e^- \rightarrow H^* + H_2O(aq)$	0.44(0.10)	0.21(0.09)

[a]The most favorable reaction in each reduction stage is shown in bold red. The standard deviations derived from independent simulations are in parentheses.

The details on the simulation parameters and the CVs for free-energy calculations are in the Supporting Information.

Figure 3 shows the lowest-energy reaction pathways for formation of both CH_4 and CH_3OH on Cu(100). The values of the free-energy differences (ΔG) and free-energy barriers ($\Delta G^{\ddagger}$) are collected in Table 1, which also lists ΔG and $\Delta G^{\ddagger}$ values for other possible side reactions.

The first reduction step is adding one H to the carbon of CO, forming chemisorbed formyl (CHO), where * indicates surface sites:

$$CO^* + H^* \rightarrow CHO^* \quad \text{(R1a)}$$

leading to $\Delta G^{\ddagger}$ = 0.55 eV and ΔG = 0.52 eV.

The alternative reaction is to form COH*. Here we examined three different mechanisms

$$CO^* + H^* \rightarrow COH^* \quad \text{(R1b)}$$

$$CO^* + (H_3O)^+ + e^- \rightarrow COH^* + H_2O \quad \text{(R1c)}$$

$$CO^* + H_2O^* \rightarrow COH^* + OH^* \quad \text{(R1d)}$$

leading to $\Delta G^{\ddagger}$ = 1.45, 0.70, and 0.74 eV, respectively. We find that the CV involves a total of 5 waters for reaction R1c and 3 waters for reaction R1d. Note that in the favored process, step R1d, it is the H_2O on the surface that transfers the proton, not the protonated H_2O.

Protonation of CHO* is easy because of the anionic character of CHO*. This leads to the second reduction step of adding H to the oxygen of CHO* to form CH−OH* as in reaction R2a

$$CHO^* + (H_3O)^+ + e^- \rightarrow CHOH^* + H_2O \quad \text{(R2a)}$$

The reaction energy barrier of 0.13 eV is consistent with previous theoretical calculations showing that free-energy barriers of proton-transfer reactions are usually between 0.15 to 0.25 eV.[50,51]

We find that surface water can also supply the H atom to form CHOH*.

$$CHO^* + H_2O^* \rightarrow CHOH^* + OH^* \quad \text{(R2b)}$$

This is favorable because after transferring the H atom, the OH product binds to Cu surface much more strongly than the reactant H_2O. This is a general phenomenon, also found in reaction R1d. The reaction barrier for reaction R2b is slightly higher, 0.24 eV. Thus, at pH 0, H_3O^+ is a better proton source than H_2O; however, in neutral and basic conditions, H_2O may provide an alternate proton source.

In addition, a competing reaction can form chemisorbed formaldehyde (CH_2=O)*.

$$CHO^* + H^* \rightarrow CH_2O^* \quad \text{(R2c)}$$

Here the energy barrier of CH_2=O formation is ΔG^{*}(R2c) = 0.59 eV, which is 0.47 eV higher than for CHOH* formation. Thus, formation of CH_2O^* is kinetically unfavorable.

Adding the third H to the oxygen of CH−OH* leads to formation of the CH--H_2O* complex

$$CHOH^* + (H_3O)^+ + e^- \rightarrow CH^*\text{--}(OH_2) + H_2O \quad \text{(R3b)}$$

which has a strong donor−acceptor bond from H_2O to the CH*. This has $\Delta G^{\ddagger}_{R3b}$ = 0.32 eV. However, dehydrating this complex to form CH* + H_2O has a barrier of 0.21 eV, leading to a net barrier of 0.53 eV (0.32 + 0.21) to form CH*.

DOI: 10.1021/acs.jpclett.5b02247
J. Phys. Chem. Lett. 2015, 6, 4767−4773

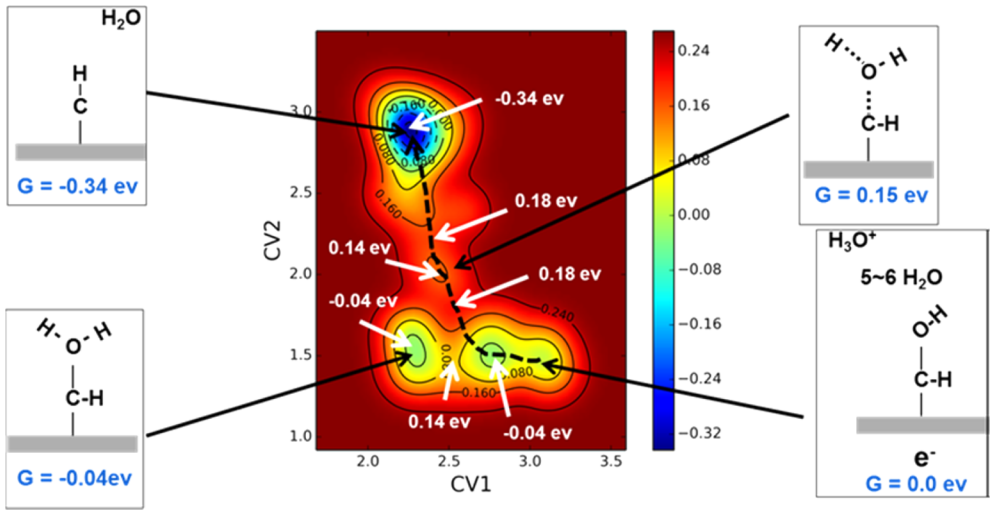

Figure 4. Two-dimensional free-energy plot for reaction R3a in Table S1 [CHOH* + $(H_3O)^+$ + e^- → CH* + H_2O(aq)]. Here CV1 is the HB network connecting H_3O^+ and CHOH with CV1 = 3.22 corresponding to $(H_3O)^+$ + CHOH and CV1 = 2.38 corresponding to H_2O + CH−H_2O. CV2 is the distance between C and H. The reactants (CHOH + H_3O^+), products (CH* + H_2O), and intermediates (CH---H_2O and CH---OH---H) are shown for viewing convenience. This concerted pathway leads to a $\Delta G^{\ddagger}_{R3b}$ = 0.30 eV [0.22 eV + 0.08 eV (constant potential correction in Table S2)].

Instead of this two-step process, we found a concerted pathway (Figure 4) that allows the dehydration to occur simultaneously as the H approaches the oxygen:

$$CHOH^* + (H_3O)^+ + e- \rightarrow CH^* + H_2O \quad \text{(R3a)}$$

Leading to a reaction barrier of 0.30 eV.

Alternatively, the third hydrogen can attack the carbon of CH−OH

$$CHOH^* + H^* \rightarrow CH_2OH^* \quad \text{(R3c)}$$

with $\Delta G^{\ddagger}_{R3c}$ = 0.45 eV. At 298 K, this reaction would be about 300 times slower than R3a.

The most plausible way to form CH_3OH from CO on Cu(100) is to add H* to CH_2−OH

$$CH_2OH^* + H^* \rightarrow CH_3OH(aq) \quad \text{(R4b)}$$

However, this leads to $\Delta G^{\ddagger}$(R4b) = 1.00 eV. Thus, both reactions R3c and R4b make CH_3OH production quite unfavorable under these conditions.

After formation of CH*, the reactions to form CH_4 are straightforward, with H adding to carbon sequentially to form CH_2*, CH_3*, and finally CH_4. All three steps are exothermic with ΔG = −0.14, −0.35, and −0.96, respectively. The energy barriers of these reactions are 0.58, 0.64, and 0.48 eV, respectively.

$$CH^* + H^* \rightarrow CH_2^* + H^* \rightarrow CH_3^* + H^* \rightarrow CH_4 \quad \text{(R4a, R5, R6)}$$

Because CH* is eventually reduced to CH_4, CH−OH* is the common intermediate at which the production of CH_4 and CH_3OH branch. However, under the current conditions, CH_4 formation is far more favorable than CH_3OH formation by a factor of 300. This is consistent with experiment: CH_4 is the only major product under acid conditions, with at most trace amounts of CH_3OH produced.[8]

The hydrogen evolution reaction is a competing reaction consuming the hydrogen required for CORR. We calculate $\Delta G^{\ddagger}$ = 0.44 eV and ΔG = 0.21 eV for the Volmer reaction (H_3O^+ + e^- → H* + H_2O), which are and consistent with experiments showing that the onset overpotential for HER is between −0.10 and −0.45 V on Cu(100).[8,52] Because $\Delta G^{\ddagger}$ and ΔG of the HER are lower than those of CH_4 formation, H_2 will evolve at a lower potential than CH_4. To suppress HER, one might change the morphology or alloying of the catalyst or introduce an adsorbate to compete with H adsorption, which are believed to be useful methods.[10,53]

Solvation effects play a major role in determining rates and selectivity. Indeed, methanol is the major product in gas-phase synthesis,[54] whereas methane is dominant for aqueous electrochemical reduction. Here the effects of solvent arise both from direct solvation (which can be included in implicit solvation models) and from formation of HBs between the surface species and the solvent molecules, which are likely not included in the solvation models. Moreover the process of providing the proton from solvent H_3O^+ or form surface H_2O involves several intermediate H_2O molecules in the H-transfer chain, which would be missing in implicit solvation models.

The solvent can also change the configuration of adsorbates on the surface. For example, the HB network generally favors orienting the C−O bond of reaction intermediates away from the surface during the whole process of CORR. Turning the C−O upside down to put the O at the surface would involve large energy barriers to break this HB network, making formation of intermediates with oxygen attached to the surface kinetically difficult. For example, our simulations indicate a small rate to form CH_3O*, even though it is energetically favorable by about 0.5 eV. This suggests that to produce methanol we should use a solvent that does *not* make strong HBs or we should change the catalyst to create a locally hydrophobic environment.

In summary, using QM with multiple layers of explicit solvent, we predict a new reaction mechanism for methane formation on Cu(100). Here there are three effects, pure solvation, specific HBs to surface OH groups, and water networks for cooperatively transferring the proton. The final mechanism for methane formation is

DOI: 10.1021/acs.jpclett.5b02247
J. Phys. Chem. Lett. 2015, 6, 4767−4773

$$CO^* \xrightarrow{H^*} CHO^* \xrightarrow{H^+ + e^-} CHOH^* \xrightarrow{H^+ + e^-} CH^* \xrightarrow{H^*} CH_2^* \xrightarrow{H^*} CH_3^* \xrightarrow{H^*} CH_4$$

where CHOH* is the common intermediate determining the selectivity of methane over methanol at low pH. The overpotential of CH_4 formation is predicted to be 0.52 V based on the free energy of CHO formation as the potential determining step, which can be compared to the experimental values of 0.45−0.50 V at low pH.[8]

■ ASSOCIATED CONTENT

Supporting Information

The Supporting Information is available free of charge on the ACS Publications website at DOI: 10.1021/acs.jpclett.5b02247.

Additional discussion of simulation methods, metadynamics, constrained molecular dynamics, collective variables, free-energy calculations, and constant potential corrections (PDF)

■ AUTHOR INFORMATION

Corresponding Author

*E-mail: wag@wag.caltech.edu.

Notes

The authors declare no competing financial interest.

■ ACKNOWLEDGMENTS

This work was initiated with support from National Science Foundation (CHE 1512759 and completed with support by the Joint Center for Artificial Photosynthesis, a DOE Energy Innovation Hub, supported through the Office of Science of the U.S. Department of Energy under Award DE-SC0004993. We thank Dr. Robert J. Nielsen, Dr. Manny Soriaga, and Ms. Yufeng Huang for helpful discussions.

■ REFERENCES

(1) Kondratenko, E. V.; Mul, G.; Baltrusaitis, J.; Larrazabal, G. O.; Perez-Ramirez, J. Status and Perspectives of CO_2 Conversion into Fuels and Chemicals by Catalytic, Photocatalytic and Electrocatalytic Processes. *Energy Environ. Sci.* **2013**, *6*, 3112−3135.

(2) Hori, Y. *Electrochemical CO_2 Reduction on Metal Electrodes*; Springer: New York, 2008.

(3) Lim, R. J.; Xie, M.; Sk, M. A.; Lee, J.-M.; Fisher, A.; Wang, X.; Lim, K. H. A Review on the Electrochemical Reduction of CO_2 in Fuel Cells, Metal Electrodes and Molecular Catalysts. *Catal. Today* **2014**, *233*, 169−180.

(4) Jones, J.-P.; Prakash, G. K. S.; Olah, G. A. Electrochemical CO_2 Reduction: Recent Advances and Current Trends. *Isr. J. Chem.* **2014**, *54*, 1451−1466.

(5) Li, Y.; Chan, S. H.; Sun, Q. Heterogeneous Catalytic Conversion of CO_2: a Comprehensive Theoretical Review. *Nanoscale* **2015**, *7*, 8663−8683.

(6) Otto, A.; Grube, T.; Schiebahn, S.; Stolten, D. Closing the Loop: Captured CO_2 as a Feedstock in the Chemical Industry. *Energy Environ. Sci.* **2015**, *8*, 3283−3297.

(7) Hori, Y.; Kikuchi, K.; Suzuki, S. Production of CO and CH_4 in Electrochemical Reduction of CO_2 at Metal Electrodes in Aqueous Hydrogencarbonate Solution. *Chem. Lett.* **1985**, 1695−1698.

(8) Schouten, K. J. P.; Pérez Gallent, E.; Koper, M. T. M. The Influence of pH on the Reduction of CO and to Hydrocarbons on Copper Electrodes. *J. Electroanal. Chem.* **2014**, *716*, 53−57.

(9) Costentin, C.; Drouet, S.; Robert, M.; Savéant, J.-M. A Local Proton Source Enhances CO_2 Electroreduction to CO by a Molecular Fe Catalyst. *Science* **2012**, *338*, 90−94.

(10) Zhang, Y.-J.; Sethuraman, V.; Michalsky, R.; Peterson, A. A. Competition between CO_2 Reduction and H_2 Evolution on Transition-Metal Electrocatalysts. *ACS Catal.* **2014**, *4*, 3742−3748.

(11) Hod, I.; Deria, P.; Bury, W.; Mondloch, J. E.; Kung, C.-W.; So, M.; Sampson, M. D.; Peters, A. W.; Kubiak, C. P.; Farha, O. K.; et al. A Porous Proton-relaying Metal-organic Framework Material That Accelerates Electrochemical Hydrogen Evolution. *Nat. Commun.* **2015**, *6*, 8304.

(12) Shi, C.; Hansen, H. A.; Lausche, A. C.; Norskov, J. K. Trends in Electrochemical CO_2 Reduction Activity for Open and Close-packed Metal Surfaces. *Phys. Chem. Chem. Phys.* **2014**, *16*, 4720−4727.

(13) Schouten, K. J. P.; Calle-Vallejo, F.; Koper, M. T. M. A Step Closer to the Electrochemical Production of Liquid Fuels. *Angew. Chem., Int. Ed.* **2014**, *53*, 10858−10860.

(14) Raciti, D.; Livi, K. J.; Wang, C. Highly Dense Cu Nanowires for Low-Overpotential CO_2 Reduction. *Nano Lett.* **2015**, *15*, 6829−6835.

(15) Li, C. W.; Ciston, J.; Kanan, M. W. Electroreduction of Carbon Monoxide to Liquid Fuel on Oxide-derived Nanocrystalline Copper. *Nature* **2014**, *508*, 504−507.

(16) Manthiram, K.; Beberwyck, B. J.; Alivisatos, A. P. Enhanced Electrochemical Methanation of Carbon Dioxide with a Dispersible Nanoscale Copper Catalyst. *J. Am. Chem. Soc.* **2014**, *136*, 13319−13325.

(17) Shen, J.; Kortlever, R.; Kas, R.; Birdja, Y. Y.; Diaz-Morales, O.; Kwon, Y.; Ledezma-Yanez, I.; Schouten, K. J. P.; Mul, G.; Koper, M. T. M. Electrocatalytic Reduction of Carbon Dioxide to Carbon Monoxide and Methane at an Immobilized Cobalt Protoporphyrin. *Nat. Commun.* **2015**, *6*, 8177.

(18) Lin, S.; Diercks, C. S.; Zhang, Y.-B.; Kornienko, N.; Nichols, E. M.; Zhao, Y.; Paris, A. R.; Kim, D.; Yang, P.; Yaghi, O. M.; et al. Covalent Organic Frameworks Comprising Cobalt Porphyrins for Catalytic CO_2 Reduction in Water. *Science* **2015**, *349*, 1208−1213.

(19) Schouten, K. J. P.; Kwon, Y.; van der Ham, C. J. M.; Qin, Z.; Koper, M. T. M. A new mechanism for the selectivity to C1 and C2 species in the electrochemical reduction of carbon dioxide on copper electrodes. *Chem. Sci.* **2011**, *2*, 1902−1909.

(20) Kuhl, K. P.; Cave, E. R.; Abram, D. N.; Jaramillo, T. F. New Insights into the Electrochemical Reduction of Carbon Dioxide on Metallic Copper Surfaces. *Energy Environ. Sci.* **2012**, *5*, 7050−7059.

(21) Reske, R.; Mistry, H.; Behafarid, F.; Roldan Cuenya, B.; Strasser, P. Particle Size Effects in the Catalytic Electroreduction of CO_2 on Cu Nanoparticles. *J. Am. Chem. Soc.* **2014**, *136*, 6978−6986.

(22) Schouten, K. J. P.; Qin, Z.; Gallent, E. P.; Koper, M. T. M. Two Pathways for the Formation of Ethylene in CO Reduction on Single-Crystal Copper Electrodes. *J. Am. Chem. Soc.* **2012**, *134*, 9864−9867.

(23) Peterson, A. A.; Abild-Pedersen, F.; Studt, F.; Rossmeisl, J.; Norskov, J. K. How Copper Catalyzes the Electroreduction of Carbon Dioxide into Hydrocarbon Fuels. *Energy Environ. Sci.* **2010**, *3*, 1311−1315.

(24) Peterson, A. A.; Nørskov, J. K. Activity Descriptors for CO_2 Electroreduction to Methane on Transition-Metal Catalysts. *J. Phys. Chem. Lett.* **2012**, *3*, 251−258.

(25) Nie, X.; Esopi, M. R.; Janik, M. J.; Asthagiri, A. Selectivity of CO_2 Reduction on Copper Electrodes: The Role of the Kinetics of Elementary Steps. *Angew. Chem., Int. Ed.* **2013**, *52*, 2459−2462.

(26) Andrews, E.; Ren, M.; Wang, F.; Zhang, Z.; Sprunger, P.; Kurtz, R.; Flake, J. Electrochemical Reduction of CO_2 at Cu Nanocluster/$(10\bar{1}0)$ ZnO Electrodes. *J. Electrochem. Soc.* **2013**, *160*, H841−H846.

(27) Kim, D.; Lee, S.; Ocon, J. D.; Jeong, B.; Lee, J. K.; Lee, J. Insights into an Autonomously Formed Oxygen-evacuated Cu_2O Electrode for the Selective Production of C_2H_4 from CO_2. *Phys. Chem. Chem. Phys.* **2015**, *17*, 824−830.

(28) Back, S.; Kim, H.; Jung, Y. Selective Heterogeneous CO_2 Electroreduction to Methanol. *ACS Catal.* **2015**, *5*, 965−971.

(29) Chen, Z.; Zhang, X.; Lu, G. Overpotential for CO_2 Electroreduction Lowered on Strained Penta-twinned Cu Nanowires. *Chem. Sci.* **2015**, *6*, 6829.

DOI: 10.1021/acs.jpclett.5b02247
J. Phys. Chem. Lett. 2015, 6, 4767−4773

(30) Hirunsit, P.; Soodsawang, W.; Limtrakul, J. CO_2 Electrochemical Reduction to Methane and Methanol on Copper-Based Alloys: Theoretical Insight. *J. Phys. Chem. C* **2015**, *119*, 8238−8249.
(31) Kim, Y.-G.; Baricuatro, J. H.; Javier, A.; Gregoire, J. M.; Soriaga, M. P. The Evolution of the Polycrystalline Copper Surface, First to Cu(111) and Then to Cu(100), at a Fixed CO2RR Potential: A Study by Operando EC-STM. *Langmuir* **2014**, *30*, 15053−15056.
(32) Hori, Y.; Takahashi, I.; Koga, O.; Hoshi, N. Electrochemical Reduction of Carbon Dioxide at Various Series of Copper Single Crystal Electrodes. *J. Mol. Catal. A: Chem.* **2003**, *199*, 39−47.
(33) Ryckaert, J.-P.; Ciccotti, G.; Berendsen, H. J. C. Numerical Integration of the Cartesian Equations of Motion of a System with Constraints: Molecular Dynamics of N-alkanes. *J. Comput. Phys.* **1977**, *23*, 327−341.
(34) Carter, E. A.; Ciccotti, G.; Hynes, J. T.; Kapral, R. Constrained Reaction Coordinate Dynamics for the Simulation of Rare Events. *Chem. Phys. Lett.* **1989**, *156*, 472−477.
(35) Laio, A.; Parrinello, M. Escaping Free-energy Minima. *Proc. Natl. Acad. Sci. U. S. A.* **2002**, *99*, 12562−12566.
(36) Iannuzzi, M.; Laio, A.; Parrinello, M. Efficient Exploration of Reactive Potential Energy Surfaces Using Car-Parrinello Molecular Dynamics. *Phys. Rev. Lett.* **2003**, *90*, 238302.
(37) Fleurat-Lessard, P.; Ziegler, T. Tracing the Minimum-energy Path on the Free-energy Surface. *J. Chem. Phys.* **2005**, *123*, 084101.
(38) van Duin, A. C. T.; Bryantsev, V. S.; Diallo, M. S.; Goddard, W. A.; Rahaman, O.; Doren, D. J.; Raymand, D.; Hermansson, K. Development and Validation of a ReaxFF Reactive Force Field for Cu Cation/Water Interactions and Copper Metal/Metal Oxide/Metal Hydroxide Condensed Phases. *J. Phys. Chem. A* **2010**, *114*, 9507−9514.
(39) van Duin, A. C. T.; Zou, C.; Joshi, K.; Bryantsev, V.; Goddard, W. A. Chapter 6: A Reaxff Reactive Force-field for Proton Transfer Reactions in Bulk Water and its Applications to Heterogeneous Catalysis; In *Computational Catalysis*; Asthagiri, A., Janik, M. J., Eds.; The Royal Society of Chemistry: Cambridge, 2014.
(40) Calle-Vallejo, F.; Koper, M. T. M. Theoretical Considerations on the Electroreduction of CO to C2 Species on Cu(100) Electrodes. *Angew. Chem., Int. Ed.* **2013**, *52*, 7282−7285.
(41) Izvekov, S.; Mazzolo, A.; VanOpdorp, K.; Voth, G. A. Ab Initio Molecular Dynamics Simulation of the Cu(110)-Water Interface. *J. Chem. Phys.* **2001**, *114*, 3248−3257.
(42) Carrasco, J.; Hodgson, A.; Michaelides, A. A Molecular Perspective of Water at Metal Interfaces. *Nat. Mater.* **2012**, *11*, 667−674.
(43) Lousada, C. M.; Johansson, A. J.; Korzhavyi, P. A. Thermodynamics of H_2O Splitting and H_2 Formation at the Cu(110)−Water Interface. *J. Phys. Chem. C* **2015**, *119*, 14102−14113.
(44) Ren, J.; Meng, S. First-principles Study of Water on Copper and Noble Metal (110) Surfaces. *Phys. Rev. B: Condens. Matter Mater. Phys.* **2008**, *77*, 054110.
(45) Jacob, T.; Goddard, W. A. Agostic Interactions and Dissociation in the First Layer of Water on Pt(111). *J. Am. Chem. Soc.* **2004**, *126*, 9360−9368.
(46) Montoya, J. H.; Shi, C.; Chan, K.; Nørskov, J. K. Theoretical Insights into a CO Dimerization Mechanism in CO_2 Electroreduction. *J. Phys. Chem. Lett.* **2015**, *6*, 2032−2037.
(47) Grimme, S.; Antony, J.; Ehrlich, S.; Krieg, H. A Consistent and Accurate Ab Initio Parametrization of Density Functional Dispersion Correction (DFT-d) for the 94 Elements H-pu. *J. Chem. Phys.* **2010**, *132*, 154104.
(48) Chan, K.; Nørskov, J. K. Electrochemical Barriers Made Simple. *J. Phys. Chem. Lett.* **2015**, *6*, 2663−2668.
(49) Mishra, H.; Enami, S.; Nielsen, R. J.; Hoffmann, M. R.; Goddard, W. A.; Colussi, A. J. Anions Dramatically Enhance Proton Transfer Through Aqueous Interfaces. *Proc. Natl. Acad. Sci. U. S. A.* **2012**, *109*, 10228−10232.
(50) Janik, M. J.; Taylor, C. D.; Neurock, M. First-principles Analysis of the Initial Electroreduction Steps of Oxygen over Pt(111). *J. Electrochem. Soc.* **2009**, *156*, B126−B135.
(51) Koper, M. M. *Molecular-Level Modeling of Anode and Cathode Electrocatalysis for PEM Fuel Cells*; Springer: New York, 2009.
(52) Brisard, G.; Bertrand, N.; Ross, P. N.; Marković, N. M. Oxygen Reduction and Hydrogen Evolution-Oxidation Reactions On Cu(hkl) Surfaces. *J. Electroanal. Chem.* **2000**, *480*, 219−224.
(53) Nørskov, J. K.; Bligaard, T.; Logadottir, A.; Kitchin, J. R.; Chen, J. G.; Pandelov, S.; Stimming, U. Trends in the Exchange Current for Hydrogen Evolution. *J. Electrochem. Soc.* **2005**, *152*, J23−J26.
(54) Studt, F.; Abild-Pedersen, F.; Wu, Q.; Jensen, A. D.; Temel, B.; Grunwaldt, J.-D.; Nørskov, J. K. CO Hydrogenation to Methanol on Cu-Ni Catalysts: Theory and Experiment. *J. Catal.* **2012**, *293*, 51−60.

DOI: 10.1021/acs.jpclett.5b02247
J. Phys. Chem. Lett. 2015, 6, 4767−4773